

Provident Vehicle Detection at Night for Advanced Driver Assistance Systems

Lukas Ewecker · Ebubekir Asan · Lars Ohnemus · Sascha Saralajew

the date of receipt and acceptance should be inserted later

Abstract In recent years, computer vision algorithms have become more powerful, which enabled technologies such as autonomous driving to evolve rapidly. However, current algorithms mainly share one limitation: They rely on directly visible objects. This is a significant drawback compared to human behavior, where visual cues caused by objects (e. g., shadows) are already used intuitively to retrieve information or anticipate occurring objects. While driving at night, this performance deficit becomes even more obvious: Humans already process the light artifacts caused by the headlamps of oncoming vehicles to estimate where they appear, whereas current object detection systems require that the oncoming vehicle is directly visible before it can be detected. Based on previous work on this subject, in this paper, we present a complete system that can detect light artifacts caused by the headlights of oncoming vehicles so that it detects that a vehicle is approaching providently (denoted as provident vehicle detection). For that, an en-

tire algorithm architecture is investigated, including the detection in the image space, the three-dimensional localization, and the tracking of light artifacts. To demonstrate the usefulness of such an algorithm, the proposed algorithm is deployed in a test vehicle to use the detected light artifacts to control the glare-free high beam system proactively (react before the oncoming vehicle is directly visible). Using this experimental setting, the provident vehicle detection system's time benefit compared to an in-production computer vision system is quantified. Additionally, the glare-free high beam use case provides a real-time and real-world visualization interface of the detection results by considering the adaptive headlamps as projectors. With this investigation of provident vehicle detection, we want to put awareness on the unconventional sensing task of detecting objects providently (detection based on observable visual cues the objects cause before they are visible) and further close the performance gap between human behavior and computer vision algorithms to bring autonomous and automated driving a step forward.

Keywords Vehicle detection · Advanced driver assistance systems · Provident object detection

1 Introduction

Humans have five senses, and, out of those, visual perception is likely to be the primary information relevant for driving a vehicle (Sivak, 1996). This fact is one reason why visual perception is essential in robots and assisted (autonomous) driving. In the last years, visual perception by machines has made tremendous progress by using Neural Networks (NNs; e. g., Deng et al., 2009; Redmon et al., 2016; Ren et al., 2015) and achieved superhuman performance for some tasks (He et al., 2016).

L. Ewecker

Dr. Ing. h.c. F. Porsche AG, Weissach, Germany. E-mail: lukas.ewecker@porsche.de

E. Asan*

Robert Bosch GmbH, Leonberg, Germany. E-mail: ebubekir.asan@bosch.com

L. Ohnemus*

Karlsruhe Institute of Technology, Karlsruhe, Germany. E-mail: lars.ohnemus@student.kit.edu

S. Saralajew*

NEC Laboratories Europe GmbH, Heidelberg, and Leibniz University Hannover, Institute of Product Development, Hannover, both Germany. E-mail: sascha.saralajew@neclab.eu

* The research was performed during employment at Dr. Ing. h.c. F. Porsche AG.

Authors contributed equally.

However, while progressing heavily in specific directions like object detection or action recognition, the abilities are far behind the general-purpose human performance, which is, for instance, reflected in the problem of adversarial robustness (e. g., Eykholt et al., 2018).

Another reason why computer vision systems cannot compete with humans in general-purpose tasks is that computer vision systems are mostly trained to solve one specific task. For this, the vision task is formulated in a mathematical framework. For example, in object detection, the most studied field in computer vision, the objects are marked by bounding boxes, and the task is to predict and classify those bounding boxes (e. g., Liu et al., 2019). Often, this sufficiently reflects our human visual performance. But, in general, human visual perception is more complex. Humans reason about the environment based on complex learned causalities using *all* the available information. If we hear a siren, for instance, we expect the occurrence of an ambulance and try to visually estimate the point of occurrence. Such causalities to enrich our environmental model are present in everyday life: In daylight, we use shadow movements and illumination changes to reason about moving objects without having direct sight, and if we drive a car through a village and see a ball rolling on the street, we expect the occurrence of playing children.

Another example for complex causalities to enrich the environmental model happens while driving at night. At night, humans show impressive abilities to foresee oncoming cars by analyzing illumination changes in the environment like light reflections on guardrails (see left image in Fig. 1), a brightening of a turn ahead, or unnatural glares in trees. Drivers use this provident information to adapt their driving style proactively, for example, by turning off the high beam in advance to avoid blinding of oncoming drivers or by adapting their driving trajectory. In the scope of safe and anticipatory driving, where time matters and the earlier information is received the better it is, this human ability is obviously handy and outperforms current computer vision systems used in vehicles. Oldenziel et al. (2020) analyzed this discrepancy between the human detection capabilities and an in-production computer vision system and quantified that humans are approximately 1.7 s faster. One reason why state-of-the-art object detection systems are behind human capabilities is that object detection systems rely on the assumption that objects have clear, visible object boundaries. Even if this assumption comes with a lot of advantages, like a well-defined description for the enclosing bounding box of an object, it is not inherently applicable to light artifacts—since usually light artifacts (illuminated areas) have no clear object boundaries and the position of these light artifacts does not directly

correspond to the location of the light source. Due to this assumption, the earliest point in time an oncoming vehicle can be detected by state-of-the-art computer vision systems is after almost full visibility (see the right image in Fig. 1).

Nowadays, vehicles are increasingly equipped with driver assistance systems, and manufacturers are working on self-driving cars. Therefore, while driving, more and more tasks are controlled or supported by systems such that the algorithms have more and more responsibility to operate correctly in our complex environment. For safe and anticipatory driving, time matters and 1.7 s are a non-negligible unexplored potential to, for instance, plan driving trajectories, understand the environment, or simply control the high beam to avoid glaring of oncoming vehicles.

In this paper,¹ we study the task of detecting *light artifacts* caused by the headlights of oncoming vehicles so that we can reduce the aforementioned time difference. To illustrate the usefulness (and to visualize the detection results in the real world and in real time), a test car is equipped with such a detection algorithm, and the information is used to proactively control the glare-free beam system² (e. g., Böke et al., 2015; Fleury et al., 2012; Kloppenburg et al., 2016). To this end, a full detection pipeline is implemented consisting of

1. the detection of light artifacts using the car’s front camera,
2. the distance estimation to all detected light artifacts to provide a three-dimensional localization, and
3. the tracking of the light artifacts to perform a plausibility check and to handle occlusions.

Consequently, by detecting their light artifacts, it is possible to detect that vehicles are oncoming before they are directly visible—this means to *providently detect oncoming vehicles*. In particular, this investigation focuses on the first two points because state-of-the-art approaches cannot be directly applied for the detection of light artifacts. Consequently, on the computer vision level, our contributions are

- a fast and straightforward computer vision algorithm that is able to detect light artifacts and

¹ Note it is the continuation of earlier work (Oldenziel et al., 2020; Saralajew et al., 2021) by our team with further improvements of the algorithm and the first detailed presentation of the entire pipeline.

² A glare-free high beam system is an ADAS where the camera interacts with a vehicle headlamp that consists of several adjustable pixels like a video projector but with a coarse resolution. By processing the information of detected vehicles of the driver assistance camera, the goal of the headlamp is to illuminate the environment as much as possible (adapted high beam) without blinding other drivers—pixels that would illuminate other drivers are turned off.

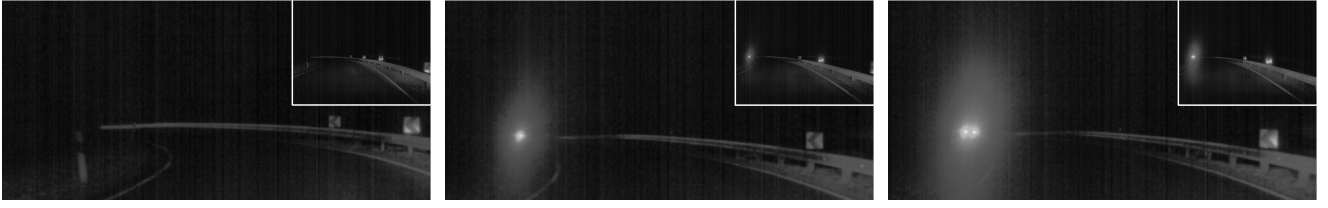


Fig. 1: The three characteristic states how an oncoming vehicle becomes visible. The images correspond to the scene 309 of the PVDN dataset (Saralajew et al., 2021). Each visualization shows a cropped area of the entire image (shown in the upper right corner). Left: First visible light artifacts at the guardrail (indirect light instance). Middle: Vehicle becomes visible (direct and indirect light instances). Right: Vehicle is visible (direct and indirect light instances).

- an investigation of methods to estimate the distance to light artifacts to estimate their three-dimensional position.

On the system level, the contributions are

- the investigation of the toolchain to integrate such a provident vehicle detection system in a vehicle to control an Advanced Driver Assistance System (ADAS) and
- the analysis of the time benefits that can be gained when using such a detection system in vehicles.

The outline of the paper is as follows: First, in Section 2, the terminology is presented that is used throughout the paper. Then, in Section 3, the current state of the art in vehicle detection at night is reviewed. This section also covers state-of-the-art methods for distance estimation for camera-based systems. Based on this, limitations of vehicle detection systems with respect to their applicability for provident vehicle detection are highlighted in Section 4. In Section 5, we present the developed provident vehicle detection pipeline. To show the feasibility of such a system in a production car environment, multiple experiments are performed in a real-world environment. The experiments are described and evaluated in Section 6, and Section 7 gives a conclusion and a future outlook.

2 Terminology

The following terminology is used:

- Light artifact: Any form of artificial light in the image caused by headlamps. This includes light reflections, glaring of areas above a street, headlamp light cones.
- Direct light instance: Light artifacts that are light sources (direct view to the headlamp).
- Indirect light instance: Light artifacts that are not direct light instances like reflections on guardrails.

Provident vehicle detection: Detect the presence of oncoming vehicles in an image (even if they are not in direct sight) by detecting light artifacts caused by the vehicle’s headlights.

Proposal generation: An algorithm to extract relevant regions (proposals) of an image in the form of bounding boxes. These regions should contain light artifacts.

Proposal classification: An algorithm to extract the proposals that correspond to *light artifacts* through classification.

Object detector: The entire detector consisting of proposal generation and proposal classification.

3 Related work

For autonomous driving and ADASs, the detection of vehicles is of high priority to perform critical tasks like emergency braking maneuvers or automatic high beam control. The commonly used sensor for that is a driver assistance camera that captures images in the visual wavelength range (e.g., Rezaei & Klette, 2017). These images are then analyzed to detect vehicles and to estimate the distance to detected vehicles to determine the three-dimensional position. The following two paragraphs present related work for these two topics (vehicle detection and distance estimation) as they are key for our contributions. Additionally, a final paragraph presents related work for provident vehicle detection.

Vehicle detection: The methods for vehicle detection by camera images depend on the visibility conditions. For example, under good visibility conditions (e.g., daylight), vehicles are detected based on feature descriptors like edge detectors and symmetry arguments using classifiers like support vector machines on top (e.g., Sun et al., 2006; Sun et al., 2002; Teoh & Bräunl, 2011) or are being detected by end-to-end trained deep NNs (e.g.,

Carranza-García et al., 2021; Fan et al., 2016; Hassaballah et al., 2021). Under this condition, detectors often assume that vehicles can be localized mainly by their contours, which is also supported by the fact that the most commonly used annotation method for objects is by bounding boxes that inherently require clearly visible object contours to reliably annotate them (see the survey of Liu et al., 2019).

If the visibility condition deteriorates, the detection performance of the aforementioned methods decreases because of the reduced visibility of object features such that specialized detection algorithms are required. For instance, for adverse weather conditions like snow or fog, Hassaballah et al. (2021) proposed a promising image enhancement strategy after which the aforementioned detectors can be applied, and, for nighttime, researchers studied whether a style transformation between nighttime and daylight images can be performed by a generative adversarial network (Lin et al., 2021; Shao et al., 2021). Even if the latter idea is promising, it is not mature enough to compete with the performances of specialized detection algorithms for nighttime (in terms of detection rates and computational efficiency).

At nighttime, due to low contrast, vehicles are usually detected by locating their headlamps and rear lights singularities in the image space caused by the luminous intensity of the light sources with rule-based algorithms (e.g., Alcantarilla et al., 2011; Eum & Jung, 2013; López et al., 2008; Pham & Yoo, 2020; Sevekar & Dhonde, 2016). However, besides rule-based approaches, methods using NNs (e.g., Bell et al., 2021; Mo et al., 2019; Oldenziel et al., 2020) or different imaging sensors like infrared cameras (e.g., Niknejad et al., 2011; Tehrani et al., 2014) have been investigated as well. For vehicle detection at night, it is difficult to judge which method is superior to another as the domain has not agreed on a benchmark dataset like the KITTI benchmark for daylight (Geiger et al., 2012), which is also criticized by other authors (Juric & Loncaric, 2014; Sun et al., 2006)—authors reported results with around 90 % accuracy and small error rates for both rule-based and NN-based classifiers on their *private* datasets (e.g., compare the evaluations of Mo et al., 2019 and Satzoda and Trivedi, 2019). Nevertheless, it has to be expected that rule-based methods are superior if computational complexity constraints apply (e.g., see the number of parameters and the number of GFLOPs in Table 2 of Saralajew et al., 2021) and if somebody wants to use the detections for high-stakes decisions (Rudin, 2019). Therefore, as the scope of this work is to apply the detection algorithm in a test vehicle for a driver assistance system, we focus on a rule-based proposal generation algorithm with a shallow NN on top to classify the pro-

posals (whereas the NN is not specific to our approach and can be replaced by any other classification method).

Distance estimation: As we consider the application of the detection pipeline in a test car to realize a prototypical customer functionality, requirements by law have to be considered. Assuming the usage of the detected vehicle information to control the vehicle’s high beams at night, the distance at which a visible vehicle must be detected is regulated by the respective UNECE Regulation No. 48 (2016) to avoid blinding of other drivers: “The sensor system shall be able to detect on a straight level road: (a) An oncoming power driven vehicle at a distance extending to at least 400 m; (b) A preceding power driven vehicle or a vehicle-trailers combination at a distance extending to at least 100 m” (Å§ 6.1.9.3.1.2).

In order to ensure such large detection distances, researchers who developed the detection pipeline for automotive use cases rely primarily on the distance estimation by a ground plane assumption (e.g., Alcantarilla et al., 2011; Y.-L. Chen et al., 2008; Eum & Jung, 2013; Juric & Loncaric, 2014; Kuo & Chen, 2010; Schamm et al., 2010).³ Knowing the extrinsic and intrinsic parameters of the camera mounted in the vehicle and assuming or estimating the ground “plane” in front of the vehicle, the distance to vehicles can be estimated. Using this technique, Alcantarilla et al. (2011) reported detection distances of up to 700 m for oncoming and 200 m for preceding vehicles. Other authors purposefully used the known calibration of the camera and different assumptions like a known distance between headlamp pairs or vanishing point estimation to estimate the distance to vehicles (e.g., D.-Y. Chen et al., 2012; Y.-L. Chen, 2009).

In addition to the methods mentioned before, researchers investigated single image depth estimation approaches by the use of deep NNs (e.g., Eigen et al., 2014; Laina et al., 2016), where the idea is that deep NNs can learn to contextualize a scene and the arrangement of objects to the depth information. Often these methods only return relative depth information that is only accurate in the close range so that it might not be applicable for our purpose. Another approach is depth estimation by structure from motion (e.g., Furukawa et al., 2004; Gallardo et al., 2017; Saponaro et al., 2014), where the structure (depth) is estimated by analyzing the movement of objects. In principle, this is similar to the distance estimation by stereo vision

³ Note that other sensors like radar and LiDAR (even if progressing constantly) cannot provide a reliable distance estimation up to such large distances (e.g., see the range specifications by Kukkala et al., 2018). In addition, a single sensor solution is also preferred in the context of low-cost solutions.

systems (Hamzah & Ibrahim, 2016) because, in both approaches, correspondences between images have to be found and analyzed. However, the latter is not applicable for our use case since we focus on monocular camera systems. Finally, in general, several of the mentioned concepts are used in depth estimation from video (e.g., Gordon et al., 2019; Ranftl et al., 2016; Zhou et al., 2017), where the goal is to provide an accurate distance estimate by analyzing consecutive images of a video.

In summary, all these methods have pros and cons and require certain assumptions to be valid. Therefore, we discuss their applicability for our use case in the following sections and, additionally, investigate a use case specific approach that uses predictive street data in order to locate light artifacts.

Provident vehicle detection: The provident detection of objects was already studied by other authors: In daylight, Naser (2019) providently detected objects by analyzing shadow movements; At nighttime, Oldenziel et al. (2020) and Saralajew et al. (2021) studied the task to providently detect oncoming vehicles by detecting light artifacts produced by their headlights.

Oldenziel et al. (2020) analyzed the discrepancy between the human abilities and an in-production computer vision system in detecting oncoming vehicles. Notably, based on the results of a test group study, the authors specified the deficit in detecting oncoming vehicles providently by 1.7 s on average in favor of humans. Since this is a significant amount of time, the authors studied whether it is possible to detect oncoming vehicles based on light artifacts by training a Faster-RCNN architecture (Ren et al., 2015) on a small private dataset annotated by bounding boxes. The presented results showed that the NN learned the task to some extent. However, the analysis of the detection results raised concerns whether an annotation method with bounding boxes (even if most commonly used) is a good annotation scheme for light artifacts due to a high annotation uncertainty because of unclear object boundaries—light artifacts are fuzzy and of weak intensity such that clear boundaries are missing. These results are partly orthogonal to Bell et al. (2021), where the authors annotated vehicles in nighttime images of traffic surveillance cameras with *keypoints* because the blurry edges of the vehicles due to motion blur and the saturated pixels due to the bright light cones of vehicles headlamps did not allow a reliable annotation of the vehicles by bounding boxes.

The annotation by keypoints causes the difficulty that the majority of state-of-the-art object detectors cannot be applied because they require bounding boxes (e.g., Liu et al., 2019). For this reason, Bell et al. (2021)

used foveal classifiers (a set of classifiers where each classifier is trained to provide the classification result for a particular image region). The disadvantage of this approach is that the localization performance depends on the number of classifiers and their distribution over the image. For their use case (traffic surveillance), however, this approach is feasible and provides good results. But for the application of provident vehicle detection, the limited localization performance and the dynamics of oncoming vehicle scenarios are expected to negatively affect the applicability of this detection approach. To overcome this and to apply state-of-the-art object detectors, the authors proposed a simple transformation by sampling bounding boxes of random size around each keypoint in order to derive bounding boxes. Based on this, they trained a YOLOv3 (Redmon & Farhadi, 2018) and a Faster R-CNN network, but these networks scored worse than their foveal classifier in the presented evaluation. Whether this result is partly due to the simplicity of their bounding box generation, perhaps causing unexpected biases, is unclear.

Saralajew et al. (2021) extended the work of Oldenziel et al. (2020) and published the PVDN dataset, the first containing approximately 60 K driver assistance camera images (grayscale) annotated by keypoints for the task to providently detect oncoming vehicles at nighttime. Together with the dataset published by Bell et al. (2021), these two datasets are the only large-scale datasets publicly available for the detection of vehicles at nighttime and annotated by keypoints—other *available* datasets for this task use bounding boxes (e.g., Duan et al., 2018; Rezaei & Klette, 2017) or masks (Rapson et al., 2018). By using keypoints for the annotation of light artifacts, Saralajew et al. (2021) presented an approach to reliably annotate light reflections, which are so fuzzy and weak in intensity that they cannot be objectively annotated by bounding boxes (as concluded by Oldenziel et al., 2020 and showed in a test by Saralajew et al., 2021). Similar to Bell et al. (2021), using the keypoints as initial seeds, the authors further explored methods to extend the keypoint annotations to bounding boxes with low annotation uncertainty so that state-of-the-art object detection methods can be applied. To this end, they trained several machine learning algorithms for the task of detecting light artifacts. The two types of architectures used for this experiment are YOLOv5 networks⁴ and a two-phase algorithm consisting of a rule-based blob detector followed by a shallow NN. Both methods show promising results and provide a strong baseline for further experiments. As mentioned earlier, we build on the latter and fine-tune the architecture such that a new benchmark is achieved.

⁴ <https://github.com/ultralytics/yolov5>

4 Inherent limitation of current systems

Simply said, the motivation of this work is to provide the information about oncoming vehicles at night earlier than current systems do—in the best case before they are directly visible—to ensure safe and anticipatory driving. Currently, there is a technical limitation in current systems regarding how early they can perceive a vehicle (see Fig. 2), caused by the commonly used object detection paradigms and the system-related latencies. Within this section, we explain why these limitations exist and are inherent. Knowing these limitations is essential to understand what can be achieved with the presented approach (how fast can vehicles be detected).

4.1 Object detection paradigms

First, it must be noted that current camera-based perception models used to detect vehicles at night are object detectors. As the most reliable information source, headlamps of other vehicles are used to detect the position of vehicles. Consequently, headlamps are used as “objects” from which succeeding systems can infer the location of vehicles present in the image (e.g., Alcantarilla et al., 2011). While being a robust reference, the restriction on headlamps limits the performance of such systems, since the earliest point in time they can perceive a vehicle is when they have direct sight to the vehicle (see “object becomes visible” in Fig. 2 and the middle image in Fig. 1). As already mentioned in Section 1, this differs from how humans estimate whether and where a vehicle is oncoming because humans can react to light artifacts like the light reflections on the guardrail in Fig. 1. Thus, the question is why light artifacts are not naturally being detected or tried to being detected by current vehicle detection systems considering the apparent discrepancy between humans and systems regarding this task (see the time gap between the human provident and camera-based object detection in Fig. 2). We can only speculate why this is the case but expect that one reason is the object detection paradigm: The algorithms detect objects that match an object definition. For example, if the object detector is a bounding box regressor, it must be possible to specify the object boundaries to define bounding boxes. In vehicle detection at night, it is possible to apply this strategy for headlamps (direct light instances) as they cause intensity singularities in the image (extraordinary high-intensity peaks) with sharp gradients. However, for light reflections (indirect light instances), this strategy is not appropriate since they often illuminate almost homogeneously larger areas with small gradients, and their intensity varies heavily depending on their strength and other global light sources.

Therefore, indirect light instances cannot be treated as objects without further thoughts due to their unclear object boundaries, causing annotation difficulties. Building on the work of Saralajew et al. (2021), we tackle this challenge by using keypoint annotations to derive a suitable object detector for detecting all sorts of light artifacts.

4.2 System-related latencies

As already mentioned in Section 3, Oldenziel et al. (2020) presented the results of a test group study that investigated the detection latency of an in-production computer vision system and humans—the results are summarized in Fig. 2. In particular, they observed that even if, in theory, detection systems are able to detect vehicles directly after direct sight, on average, they have a system-related latency. This latency is caused by a small delay until the object paradigm is fulfilled, by the image processing steps of the detection pipeline (as described in Section 1), and by the time needed to perform the plausibility check. In summary, the following steps cause the latency in a vehicle detection system—which is also qualitatively visualized in Fig. 2:

1. After the vehicle starts to become visible, there is a system-specific time until the vehicle has a visibility status that fulfills the object definition. After that, the object can be potentially detected by the computer vision system (compare the middle and right image in Fig. 1).
2. If an image is captured with an object that fulfills the object definition, a latency in the detection is caused by the image processing time (object detection, distance estimation, and tracking). This latency is lower than the frame rate of the camera.
3. Finally, the plausibility check causes a latency of several frames due to semantic and *temporal* object validations. This step is often performed in combination with the object tracking in order to safely predict there is an oncoming vehicle.

This latency is frequently discussed in combination with glare-free high beam systems because of the possible caused glare (e.g., Helmer, 2020, Chapter 3.3.1): Hummel (2009, Chapter 5.4.3) reported that the plausibility check causes a latency between two and four frames, where a frame has a processing time of 45 ms, and measured a delay from capturing the image until the high beam adapted of (196 ± 21) ms.⁵ Totzauer (2013, Chapter 3.2.4) reported a similar result of (288 ± 17.4) ms total system delay. Moreover, López et al. (2008) reported

⁵ Unless otherwise specified, expressions such as 196 ± 21 represent a mean of 196 with a standard deviation of 21.

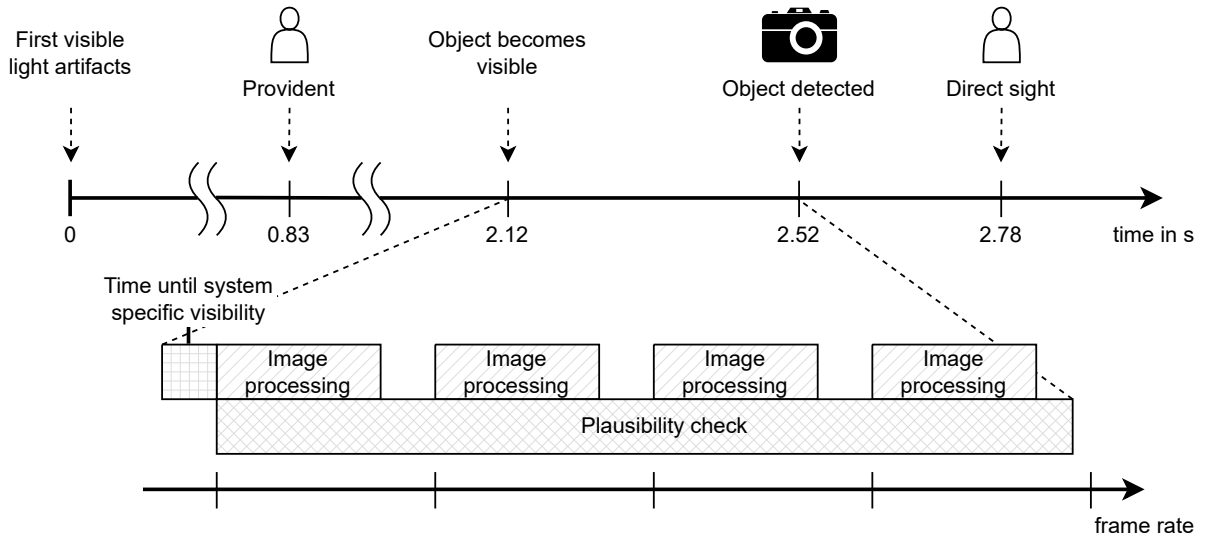


Fig. 2: Visualization of the timings of how an in-production system and humans (provident and after direct sight) perceive oncoming vehicles at night. The times are estimates from a test group study performed by Oldenziel et al. (2020) and are (of course) dependent on the scenario. However, they illustrate the inherent discrepancy. Additionally, the system-related latency between “object becomes visible” and “object detected” is qualitatively split into the single steps.

a validation time of two or three frames for oncoming vehicles. Unfortunately, they do not specify the camera’s frame rate, so these results cannot be converted into seconds. However, they state that the overall processing delay is less than 200 ms. The approach of Alcantarilla et al. (2011) validates detected vehicles for five frames at a frame rate of 30, leading to a minimum delay of around 167 ms. Summarily, current camera-based systems for detecting vehicles at night are expected to have an inherent detection delay caused by the mandatory vehicle validation procedure and the assumption that vehicles are characterized solely by headlights (as discussed in the previous Section 4.1). Consequently, if such a vehicle detection system is used to deploy a glare-free high beam system, it has to be expected that oncoming drivers are exposed to high beam light patterns when they appear in direct sight. Whether these glare moments are critical has not yet been conclusively clarified (Helmer, 2020).

Not only object detection systems have an internal latency, but also humans: reaction time. In Fig. 2, the human reaction times during the test group study are illustrated. As Oldenziel et al. (2020) showed, the camera-based vehicle detection is approximately 200 ms faster in a fair setting (allowed detection after direct sight) than its human counterpart. However, human detection almost reaches the minimal possible detection time, acting only approximately 800 ms after the first indication of oncoming vehicles (compare with the reaction times for braking maneuvers Green, 2000).

In Section 5, we present a detection system that is able to detect light artifacts. Even if this system reacts to light artifacts, it still has the inherent system-related latency. Therefore, depending on the scenario, it does not necessarily detect oncoming vehicles before direct sight but shifts as much as possible of the inherent latency before the moment of direct sight and, thus, detects oncoming vehicles faster than current systems do.

5 Method

In this section, the methodology for the detection of light artifacts is presented. First, an object detector is proposed that can detect light artifacts. After that, different techniques to estimate the distance are described. Such a distance estimation is needed to locate the detected objects in the three-dimensional space. Finally, a tracking algorithm is outlined to stabilize the detections and to perform a plausibility check.

5.1 Object detector

The first element in the vehicle detection pipeline is the object detector. The task here is to detect both direct and indirect light instances within the camera image. The feasibility of the light artifact detection was shown by Oldenziel et al. (2020) through multiple practical

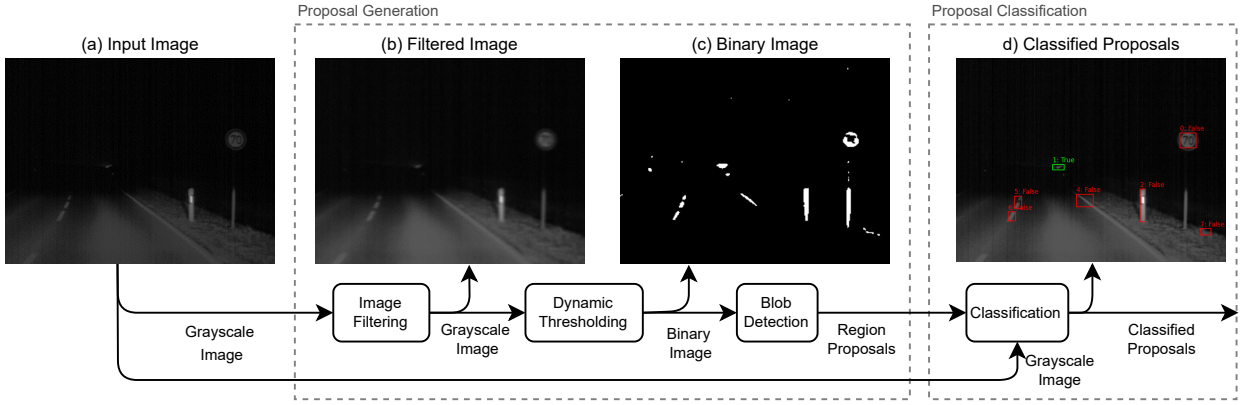


Fig. 3: Overall object detector pipeline. First, region proposals for light artifacts are generated using a custom approach described by Saralajew et al. (2021) (“Proposal Generation”). The region proposals are then passed to a classifier (“Proposal Classification”) for the binary classification to “light artifact” and “non-light artifact.” For both steps, modules, as well as intermediate results (images), are shown. Image (a) shows the raw input image, (b) the filtered image, (c) the binary image inferred through the adaptive thresholding procedure (white: 1; black: 0), (d) the classified proposals (green: light artifact, red: non-light artifact). The image used for this figure corresponds to a crop of image number 98 768 of sequence 286 in the PVDN dataset and shows the detection of an indirect light instance.

examples. The general setup for such a detector can be divided into the following sub-tasks:

1. Generate region proposals based on local features;
2. Classify the proposals to reduce the amount of false-positive detections.

This pipeline is used in many state-of-the-art systems as well as in machine learning object detectors (e. g., Ren et al., 2015). The usual approach for such a system would be to use an NN-based system in an end-to-end manner. As already said, we rejected this approach because of its inevitable obscure nature and computational load. Instead, the method proposed by Saralajew et al. (2021) with a tailored region proposal generation algorithm and an NN classifier is used. The resulting overall pipeline is depicted in Fig. 3. In the following paragraphs, each module of the object detector is described in more detail.

Pipeline: First, a dynamic thresholding procedure is performed to retrieve intensity regions of interest from the image. Bounding box proposals are then inferred through a blob detection in the generated binary image (1: above threshold; 0: below threshold). The classification is performed using a small Convolutional NN (CNN). The results are bounding box representations of light artifacts within the image.

Image preparation—The raw image is filtered to reduce the amount of noise present. First, the image size is decreased to half (640×480 pixels) by a bilinear interpolation in order to suppress small noisy image

regions (it also reduces the computational complexity of the later steps). Second, noise is further removed by applying a Gaussian blur over the entire image. This smooths out edges and removes high-frequency noise like salt-and-pepper noise. The effects of the filtering are depicted in Fig. 3b.

Dynamic thresholding—Due to the low intensities for light reflections and glares, a global thresholding strategy is not suitable to retrieve interesting regions from the raw image. In contrast, all considered artifacts share the common feature of a higher intensity relative to their surroundings (Saralajew et al., 2021). This can be used to perform dynamic thresholding on the image. Therefore, a pixel-wise threshold is calculated to retrieve interesting regions.

The criterion for the dynamic threshold $T(x, y)$ at pixel (x, y) is defined as the following:

$$T(x, y) = \mu(x, y) \cdot \left(1 + \kappa \cdot \left(1 - \frac{\Delta(x, y)}{1 - \Delta(x, y)} \right) \right), \quad (1)$$

with $\mu(x, y)$ being the local mean intensity—calculated over a fixed-sized window w around the pixel (x, y) —and $\Delta(x, y) = I(x, y) - \mu(x, y)$ being the deviation of the pixel intensity $I(x, y)$ from the local mean. The sensitivity of this threshold can be adjusted using the factor $\kappa \in \mathbb{R}$. Equation (1) is adapted from Singh et al. (2011), who originally developed this technique to binarize documents. Comparisons with other threshold techniques showed that this method yields high-quality results. Also, by using the integral image to compute the

local means, this method can be efficiently implemented (Singh et al., 2011). The threshold $T(x, y)$ is calculated for every pixel in the filtered image and used to infer a binary image $B(x, y)$ with

$$B(x, y) = \begin{cases} 1 & \text{if } I(x, y) > T(x, y), \\ 0 & \text{otherwise.} \end{cases} \quad (2)$$

An example of such a binary image is shown in Fig. 3c.

Blob detector—The binary image contains multiple, unconnected regions generated by the thresholding step. For ease of use and further handling, these regions are compressed into bounding boxes. This is achieved by applying a standard blob detection routine to find connected areas and allowing gaps of the size d —measured with respect to the L_∞ distance.⁶ After the bounding boxes have been computed, they are filtered by removing bounding boxes where the mean absolute deviation of the included intensity values is smaller than a threshold s .

Classification—The bounding boxes still contain many false positives because, simply put, all bright areas of the image are detected. This allows for a high recall of interesting regions but also yields a low precision and therefore reduces the quality of following modules (e.g., the glare-free high beam functionality). Therefore, a shallow NN is added to classify each of the proposals (this strategy is similar to a Faster-RCNN architecture). For that, to provide context information for each bounding box, an *enlarged* region around each proposal bounding box is passed through a CNN. The network classifies the proposal to be either true positive or false positive (see also Section 6.2 for a formal definition of true and false positive), leading to a binary classification problem. Here, a proposal is considered true positive if it coincides with a light artifact (direct or indirect) of oncoming vehicles. Therefore, false-positive proposals are all remaining regions. The reason for posing this as a binary classification problem is explained in more detail in Section 6.1. As the network architecture is equivalent to Saralajew et al. (2021), we will not discuss the classifier architecture in detail. For more information, see Saralajew et al. (2021) or the publicly available implementation in the corresponding GitHub repository.

Efficiency: The approach used to detect light artifacts was chosen to allow for a suitable implementation in a production car, where only limited computational resources are available. While many detection and recognition systems designed for the automotive context rely

heavily on parallel computing (e.g., through GPUs, TPUs), such hardware is not yet implemented in most production cars, limiting the practical usage of these systems. Even if more and more computational power is available in the upcoming years, resources will always be limited as the number of functions increases as well. Therefore, two of the major requirements for the detection system are to be computationally efficient and to not rely too heavily on additional hardware. The simple operations used to build the proposal generation are a result of these requirements. The classification is still performed on a GPU but is still efficient enough to be implemented on a production car’s hardware with only minor adjustments. As shown in literature, end-to-end learned systems outperform conventional methods like the proposed one. This is also partly true for our case when computational resources are unlimited. However, this fact changes with the constraint of limited computational resources, as shown by the evaluation in Section 6.2.

5.2 Distance estimator

In real-world driving scenarios, it is often not sufficient to just provide the spatial information of the detected object in the two-dimensional image space. Only knowing *where* the object of interest is located in the environment enables the vehicle to react appropriately—for example, for performing emergency brakes or adjusting the adaptive high beams. Therefore, it is necessary to compute an estimate for the three-dimensional position of detected light artifacts.

As discussed in the related work in Section 3, in the literature, there are several methods described to perform the distance estimation⁷ to locate objects. However, the special use case of nighttime images captured by a monocular grayscale camera adds clear restrictions. The general problem is that the images are relatively dark and low-textured (e.g., see Fig. 1), which complicates the application of state-of-the-art depth estimation methods. Also, light reflections can be considered non-rigid, arbitrarily deforming objects over time. In addition, the overall goal of running the method in real-time places a constraint on computational complexity, and the goal of using it for a real-world use case requires a certain range.

Table 1 presents a summary of possible applicable distance estimation methods. Due to the aforementioned constraints, the applicability of depth estimation from video and structure from motion is not possible. Additionally, monocular, single image depth estimation

⁶ The L_∞ distance, also denoted as the Chebyshev distance, between two vectors \mathbf{x} and \mathbf{y} is the maximum absolute deviation in any dimension: $L_\infty(\mathbf{x}, \mathbf{y}) = \max_i |x_i - y_i|$.

⁷ Also referred to as object localization or depth estimation.

Table 1: Summary of methods for monocular visual distance estimation (three-dimensional object localization). All methods are analyzed and assessed regarding their applicability to low-texture and dark images, computational complexity, applicability to arbitrarily deforming objects (such as light artifacts), and large distances according to the requirements discussed in Section 3.

Method	Low-textured, dark image	Arbitrarily de- forming objects	Computational complexity	Large distances
Monocular, single image depth estimation (e. g., Eigen et al., 2014; Laina et al., 2016; Wofk et al., 2019)	no	yes	high	no
Depth estimation from video (e. g., Gordon et al., 2019; Ranftl et al., 2016; Zhou et al., 2017)	no	no	high	no
Structure from motion (e. g., Furukawa et al., 2004; Gallardo et al., 2017; Saponaro et al., 2014)	partly	partly	high	no
Ground plane approaches (e. g., Alcantarilla et al., 2011; Eum & Jung, 2013; Juric & Loncaric, 2014)	yes	yes	low	yes

approaches have a too high computational complexity and cannot provide the required range, so they cannot be used for the studied approach as well.⁸ Hence, the only applicable state-of-the-art method is the object localization through ground plane approaches. Note that this method assumes that *an object is located on the ground plane*, which is not necessarily true for light artifacts (e. g., a light artifact on a guardrail). In previous work about vehicle detection where the vehicle’s headlamps are detected (e. g., Alcantarilla et al., 2011), the fulfillment of this assumption is achieved by assuming a fixed, known height of the headlamps and by shifting the ground plane by this height.

To overcome the limitations of the methods listed in Table 1, we also evaluated a rather unconventional method for estimating the distance of light artifacts by fusing the position of the object in the image with Predictive Street Data (PSD). The PSD protocol contains information about the road geometry ahead of the vehicle (see Fig. 4) based on map data and GPS and is used, for instance, for advanced navigation functionalities or adaptive cruise control. With this data, the road lying ahead can be projected into the vehicle coordinate system (see Fig. 5), giving a three-dimensional representation of the road geometry. For our implementation, the road ahead described by the PSD is defined as a set of n points $\mathcal{P} = \{P_0, P_1, P_2, \dots, P_n\}$, where P_i is a point in the vehicle coordinate system lying on the

road ahead described by the PSD. A point was sampled for every meter. At the same time, knowing the intrinsic and extrinsic camera calibration,⁹ a point (x, y) in the image can be associated with a camera ray $\vec{x}(t)$ in the vehicle coordinate system (e. g., see Hartley & Zisserman, 2004). Assuming that a detected light artifact always lies on or at least close to the road, the ray $\vec{x}(t)$ and the road ahead described by \mathcal{P} are used to search for the closest point $P_i \in \mathcal{P}$ with respect to $\vec{x}(t)$, which is an intersection between the road ahead and the ray in the best case. This point is then considered as the object position in the vehicle coordinate system. The distance between a point P_i and the ray $\vec{x}(t)$ can be calculated by

$$D(\vec{x}(t), P_i) = \frac{\|(\vec{p}_i - \vec{a}) \times \vec{n}_Q\|}{\|\vec{n}\|}, \quad (3)$$

where \vec{n} and \vec{a} are the parameter vectors of the ray $\vec{x}(t) = \vec{a} + t\vec{n}$, and where \vec{p}_i is the canonical vector representation of the point P_i . With this, the closest point of the road ahead is given by

$$P^* = \arg \min \{D(\vec{x}(t), P_i) : P_i \in \mathcal{P}\}, \quad (4)$$

which determines the position of the object in the vehicle coordinate system—detected in the image at position (x, y) .

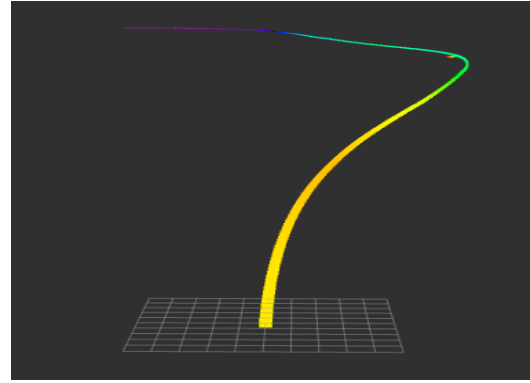
Based on the PSD data and the available ground plane approaches, the following four methods are analyzed in the experiments:

⁸ Even if these methods are not a good choice for the studied use case with respect to the computational complexity, some of them were tested in a proof-of-concept investigation on grayscale daylight and nighttime images. The results were not satisfying, which underlined the exclusion from further studies.

⁹ For in-production vehicles with a series driver assistance camera, these parameters are known and are dynamically corrected to account for vehicle dynamics and so on.



(a) Projection of the PSD road-graph into the image.



(b) Visualization of the PSD road-graph in the three-dimensional vehicle coordinate frame.

Fig. 4: Visualization of the road geometry obtained from the PSD.

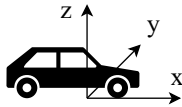


Fig. 5: Vehicle coordinate system.

PSD-3D uses the PSD road geometry (three-dimensional) and searches for the closest point along a camera ray of the detected object.

PSD-3D+ follows the PSD-3D principle but corrects the vehicle orientation (yaw angle and lateral offset) by road markers detected with the camera.¹⁰

PSD-2D follows the PSD-3D principle but simplifies the problem to a two-dimensional coordinate system by ignoring the elevation information.

GP simply assuming the road ahead as a plane (the so-called ground plane) and computing the intersection of the object's associated camera ray $\vec{x}(t)$ with the plane (e.g., Juric & Loncaric, 2014). In symbols, the ground plane is assumed to be the plane defined by $z = 0$ (see the vehicle coordinate system in Fig. 5) so that the intersection with the camera ray $\vec{x}(t)$ results from the z -components of the vectors \vec{a} and \vec{n} at the position $\vec{x}\left(\frac{-a_z}{n_z}\right)$, which determines the three-dimensional position of the object.¹¹

¹⁰ The vehicle orientation is calculated using the onboard, in-production vehicle orientation algorithm.

¹¹ Note that researchers also investigate how to improve the ground plane assumption to improve the distance estimation (e.g., Alcantarilla et al., 2011). Therefore, this simple method can be further improved.

5.3 Object tracking

The object detection and distance estimation are frame-based computations and, therefore, can be unstable with respect to the temporal context (e.g., if a vehicle gets occluded). To improve the detection stability, object tracking algorithms are used

- to match the objects between different frames,
- to predict the position of occluded objects, and
- to increase the precision of the vehicle detection.

In the literature, the dominating algorithms for this are α - β filters (e.g., López et al., 2008; Pham & Yoo, 2020) and Kalman filters (e.g., Alcantarilla et al., 2011; Teoh & Bräunl, 2011), whereas the former is a derivative of the latter. Due to the computational efficiency of the α - β filter and because good estimates for the noise covariance matrices to instantiate a Kalman filter are not known (especially for light artifacts), the proposed tracker is mainly composed of α - β filters:

- α - β filter in the two-dimensional image space to predict and estimate the position of bounding boxes;
- α - β filter to predict and estimate the distances to the objects;
- moving mean filter to estimate the confidence.

Between different frames, the object matching is performed by computing the intersection-over-union between the tracked objects and the detected objects and assigning the detected objects to the tracked objects with the highest intersection-over-union. To handle noise in the detections with respect to the bounding box size, the bounding box size of the detected objects is slightly increased before the intersection over union is computed.

If an object is occluded (not detected in the last frame), the prediction of the α - β filter is used to forecast

the position of the object for a maximal number of three frames before it is removed from the list of tracked objects. Additionally, to increase the precision of the vehicle detection system, an object is only output when it is already detected for a minimal number of five frames and if the estimated confidence is greater than a threshold of 0.5—thus, the tracker also operates as a *plausibility checker*, which is a common strategy as discussed in Section 4.2. Finally, to lower the number of tracked objects, the tracker only considers objects with a confidence value greater than 0.1.

6 Experiments

The experiments described in this section aim

- to optimize the baseline bounding box annotation quality and, therefore, the detector performance presented by Saralajew et al. (2021),
- to evaluate the distance estimation methods,
- to quantify the time benefit of the proposed system in terms of a provident detection of oncoming vehicles with respect to both human performance and an in-production computer vision system for vehicle detection at night, and
- to demonstrate the utility of the provident vehicle detection information by integrating the proposed detection system into a test car and realizing a glare-free high beam functionality.

In the following section, we describe the datasets and the test car that is used across the experiments. After that, each section describes an experiment mentioned above.

6.1 Datasets, test car, and software framework

PVDN dataset: For the evaluation of the object detector performance, the detection times, and run-times, the PVDN dataset (Saralajew et al., 2021) is used. This dataset contains 59 746 grayscale images with a resolution of 1280×960 pixels where all light artifacts—both direct (e.g., headlamps) and indirect (e.g., light reflections on guardrails)—of oncoming vehicles are annotated via keypoints. The underlying sequences of the images are recordings of test drives on rural roads with a single oncoming vehicle or multiple oncoming vehicles. Several images in the dataset include artificial light sources like street lamps that increase the difficulty of detecting light artifacts correctly. As the authors of the dataset argue, the keypoint annotations allow for an objective annotation by placing the keypoint on the intensity

maximum of each light artifact. Also, from this, an automatic generation of bounding boxes is possible, which becomes useful because most of the state-of-the-art object detectors rely on bounding box annotations. Since those bounding boxes are inferred automatically, it may happen that one bounding box covers both direct and indirect instances at the same time. This is why the task of detecting bounding boxes on the dataset is currently framed only as a binary classification problem, namely whether the bounding box covers a relevant light artifact caused by an oncoming vehicle (either direct or indirect) or not.

The images are frames of recorded video sequences so that the temporal relationships within the images of a sequence are preserved. Each scene is recorded with 18 Hz, either with a short exposure (day cycle, darker images) or long exposure (night cycle, brighter images). For the experiments in this work, the day cycle data is used as the shorter exposure results in a stronger contrast between the background and light artifacts. Within the PVDN dataset, each illumination cycle is split into a train, a validation, and a test dataset to enable the development, evaluation, and testing of algorithms. Most importantly, the sequences of the dataset contain tags that mark the timestamps where

- the oncoming vehicle is first annotated by its light artifacts,
- the driver recognized the oncoming vehicle based on its light artifacts (indirect or direct),
- the vehicle is first directly visible, and
- the in-production computer vision system first detected the oncoming vehicle.

Those tags were collected during the annotation process and the test group study, which was performed when the dataset was recorded.

Distance evaluation data: Since the PVDN dataset does not contain depth data, an additional small dataset for the evaluation of the distance estimation methods was recorded. The dataset consists of 24 scenes with 438 images in total (181 direct and 257 indirect light instances). Each scene contains five consecutive image frames to later allow for time series analyses. An exemplary sample is shown in Fig. 6. The light instances (both direct and indirect ones) were annotated manually with bounding boxes. The ground truth depth data was captured using a Hesai LiDAR sensor and the same camera system that was used to record the PVDN dataset. The single ground truth depth value for each light instance was calculated using the median of all available depth measurements within a respective bounding box.

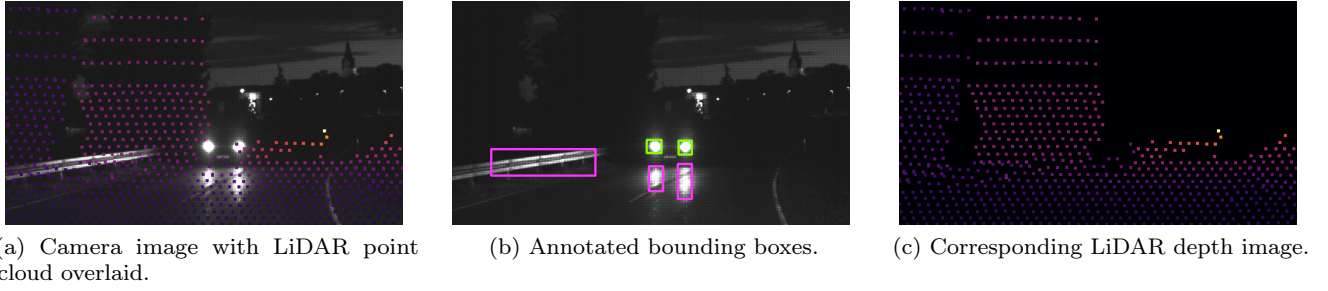


Fig. 6: Exemplary sample of the distance evaluation data. The camera image is cropped and brightness-adjusted for better visibility. The green bounding boxes mark direct and the pink indirect light instances. Black pixels in the LiDAR point cloud mean that there were no measurement points available at that location. Also, brighter points in the point cloud indicate greater distances.

Test car and software framework: A test car is used as the platform for deploying the pipeline for a real use case. It has to be noted that the test car was also used for recording the PVDN and distance evaluation dataset. Consequently, the same image input specification as for the PVDN dataset hold. Furthermore, the test car has a glare-free high beam system (Böke et al., 2015; Knöchelmann et al., 2019), which is used in the experiment for visual demonstrations and for deploying a provident glare-free high beam system. Each headlight consists of 84 LEDs, and each is almost illuminating another solid angle (within a headlight) and can be dimmed independently to all the other LEDs. Therefore, if an oncoming vehicle is detected and the glare-free high beam system is activated, the individual LEDs where the vehicle is located can be turned off such that the overall headlight system stays in “high beam mode” without blinding the oncoming vehicle—the vehicle moves in a black corridor. This corridor can be perceived by the driver, making it possible to assess the light artifact detection quality in a real environment.

To perform the experiments, an additional compute platform is used consisting of

- two Intel Xeon CPUs with a base clock frequency of 3.2 GHz and eight cores per CPU and
- one NVIDIA Tesla V100 GPU with 16 GB RAM.

The implementations on this platform are done using Python and C++ in the Melodic distribution of the Robot Operating System (ROS).¹² The ROS network consists of the following nodes connected sequentially to each other:

1. A node that receives the image task-dependent from either the driver assistance camera or from the dataset;
2. A node that detects the objects according to Section 5.1, which is internally split into two sub-nodes

where one executes the proposal generation (CPU) and one classifies the proposals by the shallow NN (GPU);

3. A node that estimates the distances to detected objects according to Section 5.2;
4. A node that performs the tracking according to Section 5.3;
5. A node that publishes the tracked objects task-dependent to either the test car’s CAN bus that controls the headlights or a buffer for further evaluations.

All nodes run single-threaded on a CPU except the shallow NN, which is executed on the GPU. With running most of the algorithm parts single-threaded on a CPU, we want to underline the transferability of the algorithms to a series platform with hardware acceleration.

6.2 Object detector

The object detector described in Section 5.1 is conceptually equivalent to the detector proposed by Saralajew et al. (2021) and consists of a rule-based proposal generation algorithm and an NN-based classifier. Originally, the parameters of the proposal generation algorithm were selected by a random search using the PVDN dataset. To improve this selection, a hyperparameter search for the proposal generation algorithm is performed using the tree-structured Parzen estimator approach (Bergstra et al., 2011). This approach belongs to the family of sequential model-based optimization approaches and is a standard algorithm for hyperparameter optimization. Before defining the objective function, the bounding box quality score and the events to define the F-score, recall, and precision is introduced (Saralajew et al., 2021): The goal of the bounding box quality score is to define a measure to assess the quality of

¹² <https://www.ros.org/>

Table 2: Parameter search space for the optimization of the bounding box annotations. The context for the specific parameters can be found in Section 5.1.

Parameter	Description	Search space	Step size	Final value
κ	Scaling parameter in dynamic thresholding.	$[0.25, 0.75]$	0.05	0.4
w	Window size in dynamic thresholding.	$\{5, 6, \dots, 25\}$	1	19
s	Threshold that the mean absolute deviation of a bounding box has to exceed to be proposed.	$[0, 0.1]$	0.01	0.01
d	Maximal L_∞ distance that is allowed between blobs to be considered in the same bounding box.	$\{1, 2, \dots, 9\}$	1	4

a bounding box prediction algorithm by using ground truth keypoints. Because each light artifact is annotated by exactly one keypoint and each bounding box should span exactly one light artifact, in the best case,

- each ground truth keypoint lies within exactly one predicted bounding box, and
- each predicted bounding box spans around exactly one ground truth keypoint.

To formalize this concept, the following events for keypoints and bounding boxes are introduced:

- True positive: The ground truth keypoint is covered by at least one bounding box (light artifact covered);
- False negative: The ground truth keypoint is not covered by any bounding box (light artifact not covered);
- False positive: The bounding box does not cover any ground truth keypoint (no light artifact covered).

By using these events, the F-score, precision, and recall can be computed. Additionally, to quantify the quality of true-positive bounding boxes, the following quantities are calculated:

- $n_K(b)$: The number of ground truth keypoints in the true-positive bounding box b ;
- $n_B(k)$: The number of true-positive bounding boxes that cover the keypoint k .

To convert these numbers into values in the range $[0, 1]$, where one means best performance and zero worst, the reciprocal value is taken. Finally, the values are averaged across the dataset to obtain measures for the performance of a detector:

$$q_K = \frac{1}{N_B} \sum_b \frac{1}{n_K(b)}, \quad (5)$$

$$q_B = \frac{1}{N_K} \sum_k \frac{1}{n_B(k)}, \quad (6)$$

where N_B is the total number of true-positive bounding boxes, and N_K is the total number of keypoints covered by bounding boxes. These two measures quantify the

uniqueness of predicted bounding boxes that are true positives with respect to how many keypoints are contained within a bounding box and how many bounding boxes cover the same keypoint. For example, in an image with several keypoints, q_K is low if a large bounding box spans over the whole image. The overall bounding box quality is determined by $q = q_K \cdot q_B$, where a value of one indicates best performance and zero worst.

Using the definition of the bounding box quality q based on the introduced events, the objective function $h(\theta)$ of the hyperparameter optimization is

$$h(\theta) = 1 - q(\theta) \longrightarrow \min, \quad (7)$$

where θ is a hyperparameter configuration. This objective function encourages bounding box generators (proposal generation algorithms) where each keypoint is uniquely assigned a bounding box. The specific search space configuration can be found in Table 2.

We optimized the hyperparameters on the official PVDN training set, selected the best parameters based on the objective function value on the validation set, and reported the results on the test set. These optimized hyperparameters were then used to generate *an optimized set of bounding box annotations for the PVDN dataset*: bounding boxes that cover a keypoint (a light artifact) were kept as ground truth bounding boxes. With these optimized bounding box annotations, the classifier was trained to distinguish between bounding boxes that contain light artifacts and bounding boxes that do not. Similar to the hyperparameter optimization, all three dataset splits of the PVDN dataset were used accordingly to train the proposal classifier. The classifier was trained for 300 epochs with an initial learning rate of 0.001, batch size of 64, weight decay of 0.01, and binary cross-entropy. Moreover, the Adam optimizer (Kingma & Ba, 2015) was used, and images were augmented with horizontal flips, rotations, crops, and gamma corrections while training. The confidence threshold for a valid classification of a light artifact was set to 0.5. To foster public use and to ensure reproduction, the whole pipeline implemented in Python with the deep learning

Table 3: Performance results of the proposed *optimized* detector, the *baseline* detector of Saralajew et al. (2021), and *YOLOv5* architectures (trained on the optimized bounding box annotations) on the PVDN day-test dataset. The values in parentheses represent the performance values of the generated bounding box annotations on the PVDN day-test dataset. These performance values for the annotations represent the maximum performance that can be achieved with the proposal generation algorithm with respect to the performance metrics. For the baseline model, the performances are reported for two different image sizes according to the published results in the GitHub repository. The run-times are measured on the specified platform without the ROS framework. For the baseline and the optimized model, the run-times are reported with standard deviations as the run-time for a specific image depends on the number of region proposals. Also, it has to be noted that the proposal generation part of the baseline and optimized model are always executed on a CPU. Acronyms: “Par.” is the number of parameters; “Prec.” is the precision.

Model	Image size	Par. [M]	Run-time [ms]	Prec.	Recall	F-score	q	q_K	q_B
Baseline	345 × 240	0.9	18.2 ± 3.3	0.88	0.54	0.67	0.40	0.40 ± 0.21	1.00 ± 0.00
		—	—	(1.00)	(0.69)	(0.81)	(0.42)	(0.42 ± 0.24)	(1.00 ± 0.00)
	640 × 480	0.9	52.71 ± 2.38	0.90	0.64	0.75	0.48	0.48 ± 0.26	1.00 ± 0.00
		—	—	(1.00)	(0.72)	(0.84)	(0.50)	(0.50 ± 0.28)	(1.00 ± 0.02)
Optimized	640 × 480	0.9	21.98 ± 1.63	0.85	0.80	0.82	0.69	0.69 ± 0.30	1.00 ± 0.02
		—	—	(1.00)	(0.87)	(0.93)	(0.70)	(0.70 ± 0.30)	(1.00 ± 0.00)
YOLOv5s	960 × 960	7.0	14.8	0.98	0.67	0.80	0.67	0.70 ± 0.31	0.97 ± 0.12
YOLOv5x		86.1	28.1	0.99	0.76	0.86	0.67	0.69 ± 0.30	0.98 ± 0.10
		—	—	(1.00)	(0.87)	(0.93)	(0.70)	(0.70 ± 0.30)	(1.00 ± 0.00)

framework PyTorch¹³ is publicly available.¹⁴ In order to make our custom detection approach comparable to state-of-the-art end-to-end object detection algorithms, we also report the performance of both YoloV5s and YoloV5x.

Table 2 shows the results of the hyperparameter optimization. Using these parameters to generate the bounding box annotations, the optimized proposal generator achieves the results reported in Table 3 (see values in parentheses). The optimized proposal generation algorithm increases the bounding box quality q from 50 % to 70 % and increases the F-score from 84 % to 93 %. Therefore, the optimized proposal generation algorithm shows a clear improvement of the automatically inferred bounding box annotations compared to the baseline. However, the performance of the optimized region proposal algorithm is still not optimal because not each performance value is 100 %. The scores which are at 100 % must be at this level due to the construction principle of the bounding boxes: Each ground truth bounding box in the generated annotations is a valid bounding box so that the precision must be 100 %; It is likely that each ground truth bounding box only covers one keypoint due to the construction of the bounding boxes by non-maximum suppression so that the quality q_B must be close to 100 %.

Because of the improved performance of the optimized proposal generation algorithm, the trained object detector shows a significant improvement of the detection performance too, as simply more of the light artifacts are captured by the proposal generation algorithm—for instance, notice the improvement of the F-score by 7 % and of the bounding box quality q by 21 %. Nevertheless, the performance values suggest that the optimized object detector can be further improved because, for example, there is a difference of 11 % between the achieved F-score and the achievable with respect to the generated optimized bounding box annotations. Considering the F-score of the two YOLOv5 variants, the optimized custom object detector is slightly superior to YOLOv5s but somewhat inferior to YOLOv5x. Moreover, the optimized object detector is marginally better with respect to the bounding box quality (achieves almost the best possible bounding box quality). The run-times of the models clearly show that YOLOv5s is the fastest detector. However, it must be noted that the optimized detector is just approximately 7 ms slower and not as optimized as the YOLOv5s architecture. The proposal generation of the optimized detector is single-threaded executed on a CPU, which is the reason why, on average, 20.55 ms of the overall run-time are consumed by this step. Therefore, it must be expected that the run-time can be greatly improved by optimizing the execution of the proposal generation step.

In summary, for embedded and safety-critical purposes, our custom approach is to be chosen before

¹³ <https://pytorch.org/>

¹⁴ <https://github.com/larsOhne/pvdn>

YOLOv5. Because it has significantly fewer parameters and thus requires less memory, and has high optimization potentials for embedded hardware. Also, the proposed optimized object detector consisting of a rule-based proposal generation algorithm and a shallow NN-classifier is more transparent than the deep NN-architectures of YOLOv5. Therefore, the approach is easier to validate and verify for safety-critical applications since the model behavior can be better understood and interpreted. Finally, we conclude that the optimized and trained light artifact detector sets a new benchmark for the PVDN dataset.

6.3 Distance estimation

This section presents the evaluation of the proposed methods of Section 5.2 on the dataset described in Section 6.1. First, the general performance of each method is evaluated on the available data. For that, each light artifact marked by a bounding box is transformed to a *single pixel by taking the center of the bounding box*. Performance results are shown in Fig. 7. It becomes clear that with a median relative error of 0.12 for direct and -0.32 for indirect light instances, the Ground Plane approach (GP), which only considers the area ahead as a plane, outperforms approaches PSD-3D, PSD-3D+, and PSD-2D, which try to estimate the road geometry using the PSD. A negative error means that the estimated distance is less than the ground truth distance. An in-depth analysis of the PSD shows that the positioning of the vehicle on the road described by the PSD is often too inaccurate to give a precise enough representation of the exact road geometry ahead, which is needed in order for the PSD approaches to work. Especially in curves, an accurate positioning of the vehicle on the road segment is absolutely mandatory since even a slight deviation can cause a considerable discrepancy between the actual road geometry ahead and the one described by the PSD at a specific time step.

When looking at the performance of the GP method, a performance deficit between direct and indirect light instances becomes clear. There are several possible reasons for this. First, the direct light instances are always located further away from the ego-vehicle than the indirect ones. The direct instances in the underlying data have an average distance of 83 m, whereas indirect instances are, on average, 63 m away. Therefore, inaccuracies influence the relative error more for the indirect instances. Second, indirect light instances often span over a large area (e.g., on the street), where the acquisition of a single ground truth distance value is difficult as the beginning of the annotated area has a different distance value than the end. This can lead to partly inaccurate

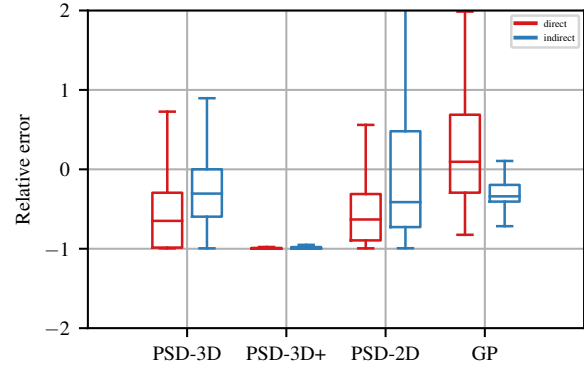


Fig. 7: Relative error results of the different methods applied on each single light artifact.

ground truth values. Third, all of the mentioned methods strongly depend on the quality of the intrinsic and extrinsic camera calibration. Thus, unknown inaccuracies in the calibration can also affect the result. Finally, the assumption of the environment ahead being a plane could often be inaccurate. If the assumption were true, the expected result for indirect light instances on the road would be nearly perfect compared to the ground truth, whereas all light instances located above the road (e.g., headlights or light reflections on guardrails) would give a too far away distance, as the camera ray would intersect with the plane behind the actual light artifact. However, the results show that the direct light instances are nearly perfect (only a little overshooting distance estimation of approximately 12 %), whereas the distance estimation for indirect instances falls too short. This indicates that the data often contains scenes where the ground plane assumption does not hold.

To investigate whether the distance estimation can be improved by considering the distance estimate of each pixel within a bounding box, several heuristics are analyzed. As the methods using the PSD already did not show satisfying results in the first experiment, the following evaluations are only done for the GP method. To retrieve the final distance estimation from all distance values within a bounding box, five simple approaches were compared with each other:

1. only considering the maximum distance value;
2. only considering the minimum distance value;
3. only considering the distance value of the lowest pixel in the bounding box (as it is closest to the estimated plane);
4. taking the mean over all distance values in the bounding box;
5. taking the median over all distance values in the bounding box.

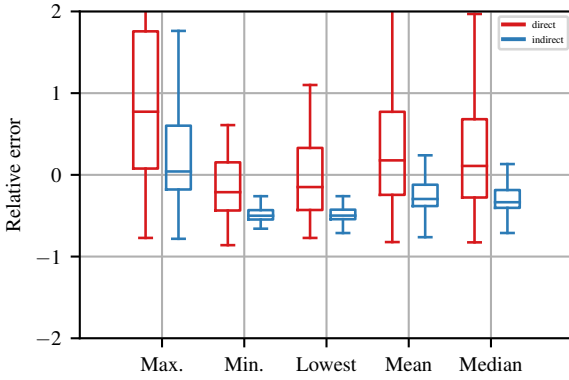


Fig. 8: Relative error results of the GP method by taking the depth values of all pixels within a bounding box into account.

The results are shown in Fig. 8. Interestingly, the five approaches do hardly show any improvements. Only the approach of taking the maximum distance value within a bounding box improves the distance estimation for indirect light instances, which makes sense considering that the original estimation for indirect light instances was often too short.

Since the annotation format of the dataset was chosen so that the correspondence of light instances across multiple frames can be determined, in a final experiment, the distance estimation for the GP method is attempted to be stabilized by considering a series of consecutive distance estimations for the same instance. The idea is that with this, possible outliers can be filtered. For that, the two approaches of taking the median or the mean of a series of distance estimations are compared. One series consists of five consecutive images. The results can be seen in Fig. 9 and do not show a significant improvement or stabilization of the distance estimations. The relative errors show an offset by roughly the same positive amount, which is a reasonable behavior since the predictions from previous time steps, where the instances were still further away, increase the final estimated distance. Note that this approach requires a tracking of detected objects across multiple images.

To summarize, the high positioning inaccuracy of the ego-vehicle on the road described by the PSD results in a highly inaccurate distance estimation of light artifacts. However, the core idea itself is promising, as it models the road environment ahead in its actual shape. Yet, the current positioning inaccuracies make the data unusable for this task. This limitation could be tackled by using high-definition maps and visual odometry to improve localization in the future. The alternative approach of modeling the world ahead as a simple plane

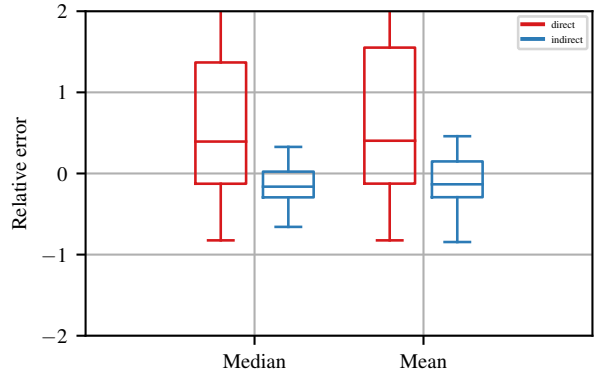


Fig. 9: Relative error results of taking the mean and the median of a series of five consecutive light artifacts.

and finding the intersection with the camera ray, however, shows satisfying results. Another advantage is that this approach does not require any sensor data except for the camera input and its calibration and also comes at a very low computational cost since calculating the intersection of a line with a plane requires only a few floating-point operations. Still, when an object is not located directly on the ground (e.g., light reflections on guardrails), the method becomes inaccurate, too. For future improvements, approaches should be analyzed that try to estimate the surface of the environment ahead in order to account for curvatures of the road surface and thus return a better approximation than the simple plane (e.g., Alcantarilla et al., 2011). However, for the system presented in this paper, the accuracy of this method is considered to be sufficient, and, therefore, the GP approach is used as the distance estimation module in our system.

6.4 Time benefit

The goal of this experiment is to evaluate the time benefit of the proposed system in terms of a provident detection of oncoming vehicles with respect to human performance and an in-production computer vision system for vehicle detection at night. For this purpose, evaluations are performed on the test and validation dataset (to increase the database) of the PVDN dataset (see Section 6.1). The sequences from the dataset are processed by the implemented ROS network, and the detection times are computed on the image frame level of the dataset. This means that the number of frames is counted between the first indirect sight annotation is available (object detectable by human annotator) and the respective system recognizing the object in the image. By knowing that the frame rate of the camera

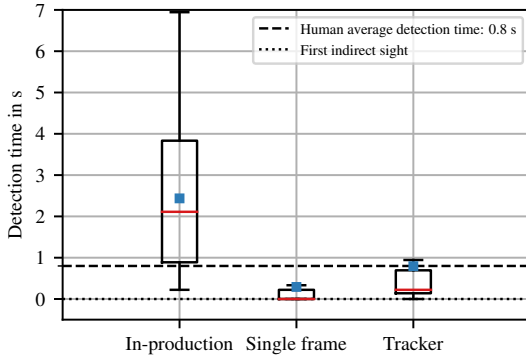


Fig. 10: Detection times of the oncoming vehicle after the first indirect sight of the in-production computer vision system, the proposed system based on single frame detections (without tracker), and with object tracking (plausibility checker). Additionally, the human detection performance is presented as a constant average value of 0.8s after the first perceivable light artifact of the oncoming vehicle (Oldenziel et al., 2020).

is 18Hz, the counted number of frames can be converted into seconds. Note that these computed times are without the system-specific processing time (see 6.5) and that the images in the dataset include a tag that specifies when the in-production system detected the oncoming vehicle. Additionally, note that even if the dataset contains images with multiple oncoming vehicles, only one can become visible first because the images are recorded on a two-lane road.¹⁵ Therefore, the number of frames is counted with respect to this first vehicle by using the available keypoint semantics (keypoints in the dataset are associated with the vehicles). In this context, the frame number when the single frame or tracking-based detection recognizes an oncoming vehicle is determined by the first bounding box that includes a keypoint associated with the first vehicle.

Fig. 10 shows the results in the form of a box plot on the respective 39 sequences of the PVDN dataset. In 18 sequences, the in-production computer vision system did not detect a vehicle and thus has fewer measurement samples. It can be seen that the proposed system based on the tracker detects oncoming vehicles, on average, 1.6s faster than the in-production computer vision system and is as fast as a human on average. The first detection based on a single frame is, on average, 2.1s before the detection of the in-production computer vision system and 0.5s before the detection of a human. The delay between the single frame detection and the tracker is caused by the plausibility phase of the tracker: an

object has to be detected for at least five frames before it is sent as output. Five frames correspond to approximately 277 ms, and this is the minimal delay inherently caused by the plausibility checker (compare with Fig. 2). Therefore, it is not surprising that the time difference between the single frame detection and the tracker is, on average, 500 ms. However, overall, the results clearly show the considerable time benefit that can be achieved by such a sensing system.

6.5 Provident glare-free high beam

To demonstrate the usefulness of the provident detection information for ADAS functionalities, we integrated the proposed detection system into the test car and used the provident detection information to control the adaptive headlights. By doing so, a provident glare-free high beam functionality is realized. The results of this experiment provide useful information about the applicability in real use cases:

- it shows that the entire workflow of the detection system can run in real time;
- it nicely visualizes the detection results in a real environment;
- it shows that glare-free high beam functions can be implemented without blinding oncoming vehicles due to latencies in the computer vision system (see Fig. 2 and discussion in Section 4.2).

The glare-free high beam functionality is suitable to visualize the detection results, as the headlights can be considered as projectors that visualize the detected objects by turning off the respective pixels. Therefore, any serious inaccuracy in the system becomes immediately visible, and thus the integration serves as a proof of concept whether the object localization uncertainties are in such a range that they still provide useful information for later systems. As already said, for this experiment, the proposed detection pipeline is integrated into the test car, and test drives are performed on *public* rural roads at night. To ensure that other drivers are not put at risk, the light artifact detection pipeline is integrated in such a way that the detection results of our pipeline are muted as soon as the in-production system detects a vehicle. Thus, the integration of the proposed pipeline just bridges the time difference between the provident detection and the in-production system. To have a unique light artifact detection output, only the detected object (after tracking) with the highest intensity value is sent to the glare-free high beam module. Because the system is tested on two-lane roads, this ensures that the detected light artifact with the highest intensity *always converges* to the vehicle’s headlamps since, after direct sight to

¹⁵ A road with one lane in each direction.

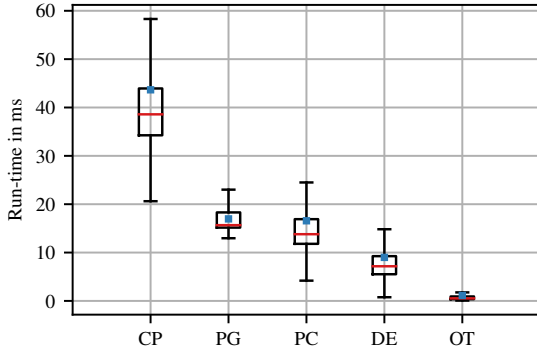


Fig. 11: Run-times of the modules (described from left to right): Run-times of the Complete Pipeline (CP), Proposal Generation (PG), Proposal Classification (PC), Distance Estimator (DE), and Object Tracker (OT).

the vehicle, the intensity maximum is in a bounding box of the headlamps. This concept circumvented the need

- to classify light artifacts into direct and indirect light instance,
- to cluster direct light instances to vehicle bounding boxes,
- to associated light artifacts to vehicles, and
- to detect occurrence points of vehicles because the proposed detection pipeline locates light artifacts.

Before the system is tested on public roads, the real-time capabilities of the pipeline are analyzed by measuring the computation times on the test car’s hardware (see Section 6.1). In this context, the run-times are determined by the elapsed time (ROS time) from receiving the node input to publishing the output. For instance, the run-time of the proposal classifier is the time from receiving the input in the form of the bounding boxes and the image until the classification of all bounding boxes is determined and published. Since the camera captures images with 18 Hz, the requirement is that the entire pipeline has an execution time faster than 18 Hz.

Fig. 11 presents the run-time analysis in the form of a box plot. The measurements were performed on the 7 030 images (test and validation dataset) of the PVDN dataset. The average run-time of the complete pipeline (entire ROS network) for one image is on average 0.044 s so that the real-time requirement is fulfilled. However, it must be noted that the run-time of the pipeline is not constant. For example, the run-time is strongly affected by the number of bounding boxes created by the proposal generator. Moreover, with an increasing number of components (after the dynamic thresholding step) during the proposal generation, the run-time of the bounding box creation (inside the proposal generator)

increases as well. Overall, the real-time requirement is fulfilled for 90 % of the analyzed images (see Fig. 11), and, therefore, the system can be deployed in the test car.¹⁶ It must be noted that the run-times of the proposal classifier and the proposal generator are different from the run-times reported in Section 6.2. This is because the evaluation here is conducted on the test and validation dataset and that the ROS framework causes a non-neglectable overhead due to data transformations to publish and process messages.

Fig. 12 shows an example scene of the test drives on rural roads at night. This scene illustrates very well the accuracy and time benefit of the proposed system in a real environment in terms of a provident vehicle detection compared to the in-production computer vision system. In Fig. 12a, the first light artifact of the oncoming vehicle can be seen. After 0.5 s, the first detection is made by the proposed system based on a single frame, as shown in Fig. 12b. Then, after 2.6 s, the tracker has validated the object and output’s it correctly to the glare-free high beam module, see Fig. 12c. Based on the result of the tracker, the end of the road is dimmed proactively (a black gap can be seen in the white box) to avoid blinding the oncoming driver. The in-production system detects the oncoming vehicle after 3.8 s when it is fully visible and after a significant latency, see Fig. 12d. Therefore, the in-production system would have caused a short glare for the oncoming driver. In this scene, there is a total time benefit of 1.2 s of the proposed system.

This experiment provides a useful visualization interface of the detection results in the real world. It also shows that despite the localization uncertainties of the proposed detector and distance estimator, the information can be used to realize a provident glare-free high beam system. However, there are two points that need to be clarified:

1. Why is the dimmed gap (see the white box in Fig. 12c) larger than the detected light reflection and tends to the left?
2. Why does the tracker take “so long” after the first detection to detect the oncoming vehicle?

First, the reason for the size of the dimmed area is due to the low resolution of the headlights (see Section 6.1), and, for safety reasons, detected objects are always increased by a safety margin inside the glare-free high beam module. Moreover, the left tendency might be caused by the inaccuracies of the distance estimation. Second, the reason for the late detection of the tracker (in this case, 2.1 s after the first detection based on a

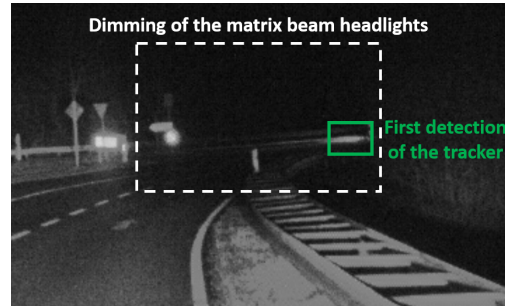
¹⁶ If the computation is still running and the camera has already captured a new image, the new camera image is dropped in the deployed algorithm.



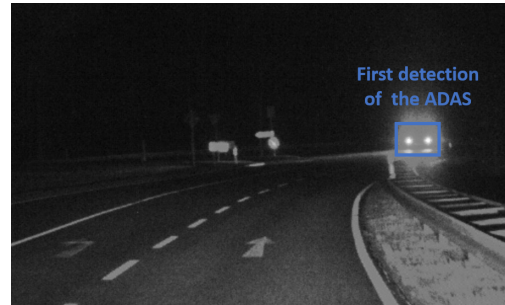
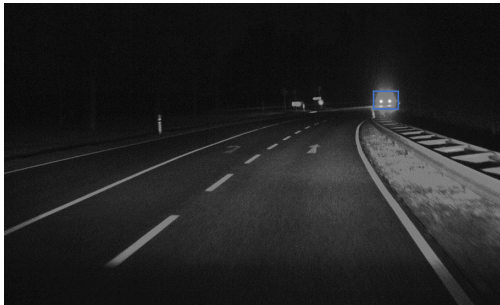
(a) First sight of indirect light instances on the guardrail between the trees.



(b) First detection of the system based on single frame detections 0.5s after first sight. The detection contains two direct instances (headlamps) as well as an indirect instance on the guardrail. Note that the entire scene is still illuminated by the adaptive headlight (see the bright lane markings and the trees).



(c) First detection of the tracker 2.6s after first sight and, the headlights dim the corresponding pixels. The system's reaction is based on the indirect light instance on the guardrail as the vehicle itself is not visible in this frame. The dimmed region is best recognized by focusing on the glow changes of the lane markings and that trees are not illuminated. Also, note how the indirect light instance with the highest intensity is at the position where the vehicle will occur, which shows how this light artifact converges to the vehicle position.



(d) First detection of the in-production system based on direct light instances 3.8s after first sight.

Fig. 12: Visual demonstration of the time benefit of the proposed system in terms of a provident vehicle detection by the glare-free high beam functionality on a recorded scene during test drives. The left images always show the full image, and the right images always show a cropped version of the full image. The upper part of all the images is cut off so that the figure fits on one page.

single frame) is because the vehicle disappears behind the trees several times, which makes it difficult for the tracker to continuously track the vehicle over multiple frames.

7 Conclusion and outlook

Extending the work of Oldenziel et al. (2020) and Saralajew et al. (2021), with this work, we presented a complete pipeline designed for automotive use cases which is capable of providently detecting vehicles at night. The system consists of a set of algorithms solving the tasks of detection, three-dimensional localization, and tracking of both direct light instances (e.g., headlights) and indirect light instances (e.g., light reflections on guardrails) caused by oncoming vehicles. The evaluation shows that this detection pipeline can detect oncoming vehicles almost 1.6 s earlier than conventional vehicle detection systems at night, which can be considered a significant amount of time for automotive use cases. Also, by deploying the pipeline in a test car for the use case of providently controlling the glare-free high beam system for oncoming vehicles, the applicability of the proposed detection pipeline is demonstrated not only under laboratory conditions but also in real scenarios and in real time.

Currently, for further use cases (e.g., trajectory planning, automatic emergency braking), the system might still lack the necessary precision in three-dimensional localization of the light reflections. Therefore, future work should focus on evaluating new distance estimation methods by extending the currently applied ground plane assumption to a more precise representation of the environmental geometry ahead. Additionally, in order to exploit the full potential of provident vehicle detection, it is necessary to address the points circumvented in Section 6.5. One of the biggest challenges in this context might be to identify the point where the oncoming vehicle might appear. In addition, future work should also investigate the applicability of the provident detection algorithm in urban scenarios (e.g., at intersections in cities). If successful, this would be an important step on the way to computer vision algorithms that resemble human perceptual capabilities.

References

- Alcantarilla, P. F., Bergasa, L. M., Jiménez, P., Parra, I., Llorca, D. F., Sotelo, M. A., & Mayoral, S. S. (2011). Automatic LightBeam controller for driver assistance. *Machine Vision and Applications*, 22(5), 819–835. <https://doi.org/10.1007/s00138-011-0327-y>
- Bell, A., Mantecon, T., Diaz, C., del-Blanco, C. R., Jaureguizar, F., & Garcia, N. (2021). A novel system for nighttime vehicle detection based on foveal classifiers with real-time performance. *IEEE Transactions on Intelligent Transportation Systems*, 1–13. <https://doi.org/10.1109/tits.2021.3053863>
- Bergstra, J., Bardenet, R., Bengio, Y., & Kégl, B. (2011). Algorithms for hyper-parameter optimization. In J. Shawe-Taylor, R. S. Zemel, P. L. Bartlett, F. C. N. Pereira, & K. Q. Weinberger (Eds.), *Advances in Neural Information Processing Systems 24: Proceedings of the Neural Information Processing Systems Conference – NIPS 2011* (pp. 2546–2554).
- Böke, B., Maier, M., Moisel, J., & Herold, F. (2015). The Mercedes-Benz headlamp of the future: Higher resolution with greater intelligence for enhanced safety. *Proc. Int. Symposium on Automotive Lighting*, 49–58.
- Carranza-García, M., Lara-Benítez, P., García-Gutiérrez, J., & Riquelme, J. C. (2021). Enhancing object detection for autonomous driving by optimizing anchor generation and addressing class imbalance. *Neurocomputing*, 449, 229–244. <https://doi.org/10.1016/j.neucom.2021.04.001>
- Chen, D.-Y., Lin, Y.-H., & Peng, Y.-J. (2012). Nighttime brake-light detection by Nakagami imaging. *IEEE Transactions on Intelligent Transportation Systems*, 13(4), 1627–1637. <https://doi.org/10.1109/tits.2012.2199983>
- Chen, Y.-L. (2009). Nighttime vehicle light detection on a moving vehicle using image segmentation and analysis techniques. *World Scientific and Engineering Academy and Society (WSEAS) Transactions on Computers*, 8(3), 506–515.
- Chen, Y.-L., Lin, C.-T., Fan, C.-J., Hsieh, C.-M., & Wu, B.-F. (2008). Vision-based nighttime vehicle detection and range estimation for driver assistance. *Proceedings of the IEEE International Conference on Systems, Man and Cybernetics – SMC 2008*, 2988–2993. <https://doi.org/10.1109/icsmc.2008.4811753>
- Deng, J., Dong, W., Socher, R., Li, L.-J., Li, K., & Fei-Fei, L. (2009). ImageNet: A large-scale hierarchical image database. *Proceedings of the 2009 IEEE Conference on Computer Vision and Pattern Recognition – CVPR 2009*, 248–255. <https://doi.org/10.1109/CVPRW.2009.5206848>
- Duan, Y., Kuang, H., Qiu, W., Chan, L. L. H., & Yan, H. (2018). Cascade feature selection and coarse-to-

- fine mechanism for nighttime multiclass vehicle detection. *Journal of Electronic Imaging*, 27(3), 1–12. <https://doi.org/10.1117/1.jei.27.3.033042>
- Eigen, D., Puhrsch, C., & Fergus, R. (2014). Depth map prediction from a single image using a multi-scale deep network. In Z. Ghahramani, M. Welling, C. Cortes, N. D. Lawrence, & K. Q. Weinberger (Eds.), *Advances in Neural Information Processing Systems 27: Proceedings of the Neural Information Processing Systems Conference – NIPS 2014* (pp. 2366–2374).
- Eum, S., & Jung, H. G. (2013). Enhancing light blob detection for intelligent headlight control using lane detection. *IEEE Transactions on Intelligent Transportation Systems*, 14(2), 1003–1011. <https://doi.org/10.1109/TITS.2012.2233736>
- Eykholt, K., Evtimov, I., Fernandes, E., Li, B., Rahmati, A., Xiao, C., Prakash, A., Kohno, T., & Son, D. (2018). Robust physical-world attacks on deep learning visual classification. *Proceedings of the 2018 IEEE/CVF Conference on Computer Vision and Pattern Recognition – CVPR 2018*, 1625–1634. <https://doi.org/10.1109/CVPR.2018.00175>
- Fan, Q., Brown, L., & Smith, J. (2016). A closer look at Faster R-CNN for vehicle detection. *Proceedings of the IEEE Intelligent Vehicles Symposium – IV 2016*, 124–129. <https://doi.org/10.1109/ivs.2016.7535375>
- Fleury, B., Evrard, L., Ravier, J.-P., & Reiss, B. (2012). Expanded functionality of glare free high beam systems. *ATZ worldwide*, 114, 44–49. <https://doi.org/10.1007/s38311-012-0179-8>
- Furukawa, Y., Sethi, A., Ponce, J., & Kriegman, D. J. (2004). Structure and motion from images of smooth textureless objects. In T. Pajdla & J. Matas (Eds.), *Proceedings of the 8th European Conference on Computer Vision Computer Vision – ECCV 2004* (pp. 287–298). Springer. https://doi.org/10.1007/978-3-540-24671-8_23
- Gallardo, M., Collins, T., & Bartoli, A. (2017). Dense non-rigid structure-from-motion and shading with unknown albedos. *Proceedings of the IEEE International Conference on Computer Vision – ICCV 2017*, 3904–3912. <https://doi.org/10.1109/ICCV.2017.419>
- Geiger, A., Lenz, P., & Urtasun, R. (2012). Are we ready for autonomous driving? the KITTI vision benchmark suite. *Proceedings of the 2012 IEEE Computer Society Conference on Computer Vision and Pattern Recognition – CVPR 2012*, 3354–3361. <https://doi.org/10.1109/CVPR.2012.6248074>
- Gordon, A., Li, H., Jonschkowski, R., & Angelova, A. (2019). Depth from videos in the wild: Unsupervised monocular depth learning from unknown cameras. *Proceedings of the IEEE/CVF International Conference on Computer Vision – ICCV 2019*, 8976–8985. <https://doi.org/10.1109/ICCV.2019.00907>
- Green, M. (2000). “How long does it take to stop?” Methodological analysis of driver perception-brake times. *Transportation Human Factors*, 2(3), 195–216. https://doi.org/10.1207/sthf0203_1
- Hamzah, R. A., & Ibrahim, H. (2016). Literature survey on stereo vision disparity map algorithms. *J. Sensors*, 2016, 1–23. <https://doi.org/10.1155/2016/8742920>
- Hartley, R., & Zisserman, A. (2004). *Multiple view geometry in computer vision* (2nd ed.). Cambridge University Press. <https://doi.org/10.1017/CBO9780511811685>
- Hassaballah, M., Kenk, M. A., Muhammad, K., & Minaee, S. (2021). Vehicle detection and tracking in adverse weather using a deep learning framework. *IEEE Transactions on Intelligent Transportation Systems*, 22(7), 4230–4242. <https://doi.org/10.1109/tits.2020.3014013>
- He, K., Zhang, X., Ren, S., & Sun, J. (2016). Deep residual learning for image recognition. *Proceedings of the 2016 IEEE Conference on Computer Vision and Pattern Recognition – CVPR 2016*, 770–778. <https://doi.org/10.1109/CVPR.2016.90>
- Helmer, M. (2020). *Methode zur Messung des Einflusses von Lichtimpulsen auf die visuelle Leistungsfähigkeit [Method for measuring the influence of light pulses on visual performance]* (Doctoral dissertation). Karlsruhe Institute of Technology. <https://doi.org/10.5445/IR/1000104719>
- Hummel, B. (2009). *Blendfreies LED-Fernlicht [Glare-free LED high beam]* (Doctoral dissertation). Karlsruhe Institute of Technology.
- Juric, D., & Loncaric, S. (2014). A method for on-road night-time vehicle headlight detection and tracking. *Proceedings of the International Conference on Connected Vehicles and Expo – ICCVE 2014*, 655–660. <https://doi.org/10.1109/iccve.2014.7297630>
- Kingma, D. P., & Ba, J. (2015). Adam: A method for stochastic optimization. In Y. Bengio & Y. LeCun (Eds.), *Proceedings of the 3rd Interna-*

- tional Conference on Learning Representations – ICLR 2015*.
- Kloppenburger, G., Wolf, A., & Lachmayer, R. (2016). High-resolution vehicle headlamps: Technologies and scanning prototype. *Advanced Optical Technologies*, 5(2), 147–155. <https://doi.org/doi:10.1515/aot-2016-0001>
- Knöchelmann, M., Held, M., Kloppenburger, G., & Lachmayer, R. (2019). High-resolution headlamps – technology analysis and system design. *Advanced Optical Technologies*, 8(1), 33–46.
- Kukkala, V. K., Tunnell, J., Pasricha, S., & Bradley, T. (2018). Advanced driver-assistance systems: A path toward autonomous vehicles. *IEEE Consumer Electronics Magazine*, 7(5), 18–25. <https://doi.org/doi:10.1109/MCE.2018.2828440>
- Kuo, Y.-C., & Chen, H.-W. (2010). Vision-based vehicle detection in the nighttime. *Proceedings of the International Symposium on Computer, Communication, Control and Automation – 3CA 2010*, 361–364. <https://doi.org/doi:10.1109/3ca.2010.5533451>
- Laina, I., Rupprecht, C., Belagiannis, V., Tombari, F., & Navab, N. (2016). Deeper depth prediction with fully convolutional residual networks. *Proceedings of the 4th International Conference on 3D Vision – 3DV 2016*, 239–248. <https://doi.org/doi:10.1109/3DV.2016.32>
- Lin, C.-T., Huang, S.-W., Wu, Y.-Y., & Lai, S.-H. (2021). GAN-based day-to-night image style transfer for nighttime vehicle detection. *IEEE Transactions on Intelligent Transportation Systems*, 22(2), 951–963. <https://doi.org/doi:10.1109/tits.2019.2961679>
- Liu, L., Ouyang, W., Wang, X., Fieguth, P., Chen, J., Liu, X., & Pietikäinen, M. (2019). Deep learning for generic object detection: A survey. *International Journal of Computer Vision*, 128(2), 261–318. <https://doi.org/doi:10.1007/s11263-019-01247-4>
- López, A. M., Hilgenstock, J., Busse, A., Baldrich, R., Lumbreras, F., & Serrat, J. (2008). Nighttime vehicle detection for intelligent headlight control. In J. Blanc-Talon, S. Bourennane, W. Philips, D. C. Popescu, & P. Scheunders (Eds.), *Proceedings of the 10th International Conference on Advanced Concepts for Intelligent Vision Systems – ACIVS 2008* (pp. 113–124). Springer, Berlin, Heidelberg. https://doi.org/doi:10.1007/978-3-540-88458-3_11
- Mo, Y., Han, G., Zhang, H., Xu, X., & Qu, W. (2019). Highlight-assisted nighttime vehicle detection using a multi-level fusion network and label hierarchy. *Neurocomputing*, 355, 13–23. <https://doi.org/doi:10.1016/j.neucom.2019.04.005>
- Naser, F. M. (2019). *Detection of dynamic obstacles out of the line of sight for autonomous vehicles to increase safety based on shadows* (Master’s thesis). MIT. Boston, Department of Electrical Engineering; Computer Science.
- Niknejad, H. T., Takahashi, K., Mita, S., & McAllester, D. (2011). Vehicle detection and tracking at nighttime for urban autonomous driving. *Proceedings of the IEEE/RSJ International Conference on Intelligent Robots and Systems – IROS 2011*, 4442–4447. <https://doi.org/doi:10.1109/iros.2011.6094830>
- Oldenziel, E., Ohnemus, L., & Saralajew, S. (2020). Provident detection of vehicles at night. *Proceedings of the 2020 IEEE Intelligent Vehicles Symposium – IV 2020*, 472–479. <https://doi.org/doi:10.1109/IV47402.2020.9304752>
- Pham, T.-A., & Yoo, M. (2020). Nighttime vehicle detection and tracking with occlusion handling by pairing headlights and taillights. *Applied Sciences*, 10(11), 1–18. <https://doi.org/doi:10.3390/app10113986>
- Ranftl, R., Vineet, V., Chen, Q., & Koltun, V. (2016). Dense monocular depth estimation in complex dynamic scenes. *Proceedings of the 2016 IEEE Conference on Computer Vision and Pattern Recognition – CVPR 2016*, 4058–4066. <https://doi.org/doi:10.1109/CVPR.2016.440>
- Rapson, C. J., Seet, B.-C., Naeem, M. A., Lee, J. E., Al-Sarayreh, M., & Klette, R. (2018). Reducing the pain: A novel tool for efficient ground-truth labelling in images. *International Conference on Image and Vision Computing New Zealand – IVCNZ 2018*, 1–9. <https://doi.org/doi:10.1109/ivcnz.2018.8634750>
- Redmon, J., Divvala, S., Girshick, R., & Farhadi, A. (2016). You only look once: Unified, real-time object detection. *Proceedings of the IEEE Conference on Computer Vision and Pattern Recognition*, 779–788.
- Redmon, J., & Farhadi, A. (2018). YOLOv3: An incremental improvement. *CoRR*, abs/1804.02767. <http://arxiv.org/abs/1804.02767>
- Ren, S., He, K., Girshick, R., & Sun, J. (2015). Faster R-CNN: Towards real-time object detection with region proposal networks. In C. Cortes, N. D. Lawrence, D. D. Lee, M. Sugiyama, & R. Garnett (Eds.), *Advances in Neural Information Processing Systems 28: Proceedings of the Neural Information Processing Systems Conference*

- *NIPS 2015* (pp. 91–99). Curran Associates, Inc.
- Rezaei, M., & Klette, R. (2017). *Computer vision for driver assistance – Simultaneous traffic and driver monitoring* (Vol. 45). Springer. <https://doi.org/10.1007/978-3-319-50551-0>
- Rudin, C. (2019). Stop explaining black box machine learning models for high stakes decisions and use interpretable models instead. *Nature Machine Intelligence*, 1, 206–215. <https://doi.org/10.1038/s42256-019-0048-x>
- Saponaro, P., Sorensen, S., Rhein, S., Mahoney, A. R., & Kambhamettu, C. (2014). Reconstruction of textureless regions using structure from motion and image-based interpolation. *Proceedings of the 2014 IEEE International Conference on Image Processing – ICIP 2014*, 1847–1851. <https://doi.org/10.1109/ICIP.2014.7025370>
- Saralajew, S., Ohnemus, L., Ewecker, L., Asan, E., Isele, S., & Roos, S. (2021). A dataset for provident vehicle detection at night. *Proceedings of the IEEE/RSJ International Conference on Intelligent Robots and Systems – IROS 2021*, 9750–9757. <https://doi.org/10.1109/iros51168.2021.9636162>
- Satzoda, R. K., & Trivedi, M. M. (2019). Looking at vehicles in the night: Detection and dynamics of rear lights. *IEEE Transactions on Intelligent Transportation Systems*, 20(12), 4297–4307. <https://doi.org/10.1109/tits.2016.2614545>
- Schamm, T., von Carlowitz, C., & Zollner, J. M. (2010). On-road vehicle detection during dusk and at night. *Proceedings of the IEEE Intelligent Vehicles Symposium – IV 2010*, 418–423. <https://doi.org/10.1109/ivs.2010.5548013>
- Sevekar, P., & Dhonde, S. B. (2016). Nighttime vehicle detection for intelligent headlight control: A review. *Proceedings of the 2016 2nd International Conference on Applied and Theoretical Computing and Communication Technology (iCATccT)*, 188–190. <https://doi.org/10.1109/ICATCCT.2016.7911989>
- Shao, X., Wei, C., Shen, Y., & Wang, Z. (2021). Feature enhancement based on CycleGAN for nighttime vehicle detection. *IEEE Access*, 9, 849–859. <https://doi.org/10.1109/access.2020.3046498>
- Singh, T. R., Roy, S., Singh, O. I., Sinam, T., & Singh, K. M. (2011). A new local adaptive thresholding technique in binarization. *IJCSI International Journal of Computer Science Issues*, 8(6), 271–277.
- Sivak, M. (1996). The information that drivers use: Is it indeed 90% visual? *Perception*, 25(9), 1081–1089. <https://doi.org/10.1068/p251081>
- Sun, Z., Bebis, G., & Miller, R. (2006). On-road vehicle detection: A review. *IEEE Transactions on Pattern Analysis and Machine Intelligence*, 28(5), 694–711. <https://doi.org/10.1109/TPAMI.2006.104>
- Sun, Z., Miller, R., Bebis, G., & DiMeo, D. (2002). A real-time precrash vehicle detection system. *Proceedings of the 6th IEEE Workshop on Applications of Computer Vision – WACV 2002*, 171–176. <https://doi.org/10.1109/ACV.2002.1182177>
- Tehrani, H., Kawano, T., & Mita, S. (2014). Car detection at night using latent filters. *Proceedings of the IEEE Intelligent Vehicles Symposium – IV 2014*, 839–844. <https://doi.org/10.1109/ivs.2014.6856518>
- Teoh, S. S., & Bräunl, T. (2011). Symmetry-based monocular vehicle detection system. *Machine Vision and Applications*, 23(5), 831–842. <https://doi.org/10.1007/s00138-011-0355-7>
- Totzauer, A. (2013). *Kalibrierung und Wahrnehmung von blendfreiem LED-Fernlicht [Calibration and perception of glare-free LED high beam]* (Doctoral dissertation). Technical University of Darmstadt.
- UNECE Regulation No. 48. (2016). *Regulation No. 48 – Uniform provisions concerning the approval of vehicles with regard to the installation of lighting and light-signalling devices* (Standard). Economic Commission for Europe of the United Nations (UNECE).
- Wofk, D., Ma, F., Yang, T., Karaman, S., & Sze, V. (2019). FastDepth: fast monocular depth estimation on embedded systems. *Proceedings of the International Conference on Robotics and Automation – ICRA 2019*, 6101–6108. <https://doi.org/10.1109/ICRA.2019.8794182>
- Zhou, T., Brown, M., Snavely, N., & Lowe, D. G. (2017). Unsupervised learning of depth and ego-motion from video. *Proceedings of the 2017 IEEE Conference on Computer Vision and Pattern Recognition – CVPR 2017*, 6612–6619. <https://doi.org/10.1109/CVPR.2017.700>